

## Solar Particle Events and Radiation Exposure in Space

Shaowen Hu (Shaowen.Hu-1@nasa.gov)

KBRwyle, Houston, TX

### Abstract

Radiation exposure from solar particle events (SPEs) presents a significant health concern for astronauts for exploration missions outside the protection of the Earth's magnetic field, which could impair their performance and result in possible mission failure. Accurate assessment on the impact of SPEs on human exploration missions remains a challenge due to incomplete understanding of many physical processes during the occurring of SPEs. This article summarizes recent observation and theoretical frameworks concerning the origin, acceleration, and transport of energetic particles in SPEs, and reviews knowledge of the sizes, frequencies, energy spectra of SPEs obtained from decades of solar physics research, as well as techniques of radiation exposure modeling relevant to interplanetary space exploration. It is expected that future close collaborations among solar, heliospheric, space weather, and radiation research communities on observational and theoretical studies will enhance the development of reliable and accurate predictive models for SPEs.

### 1. Introduction

The Sun not only constantly releases warmth and light that are essential to maintain the habitability of the Earth, but also sometimes discharge large amount of energetic particles that are hazard to human health and instruments in space. Solar particle events (SPEs), for example, occur when protons emitted by the Sun become accelerated either close to the Sun during a flare or in interplanetary space by coronal mass ejection (CME) shocks. The events can include other nuclei such as helium ions and highly charged (Z) and energetic (E) (HZE) ions. During a large SPE, the fluence of protons with energies  $>30$  MeV can exceed  $10^{10}$  cm<sup>-2</sup> in several hours or days, which can deposit large radiation doses for crew and equipment that are not adequately protected. Though such big events are rare in history, currently there are no reliable ways to predict their occurrence and give sufficient time of warning before the onset. These hazards impose significant operational constraints on manned space missions and equipment, for example, storm shelters with sufficient shielding are needed to reduce the radiation dose to tolerable levels for astronauts, and equipments sensitive to such high energy particles need to turn off to avoid soft errors or radiation damage. In the past several decades, the advance of space exploration enables scientists to use multiple spacecraft deployed in different locations in heliosphere, to study the relationship of SPE intensities and spectra with measurable parameters of the shock, plasma, seed population, and their spatial distribution, which greatly improves our understanding the conditions where, when, how, and why particle acceleration takes place in these exceptional events [Reames, 2013].

### 2. Size and Frequency of SPEs

There have been various definitions of SPEs using different parameters to extract the events from the time series, and it is generally agreed that the frequency of occurrence of SPEs varies, from several per day when the Sun is particularly "active" to less than 1 every week when the Sun is

"quiet"<sup>1</sup>, following the 11-year cycle generally divided into four inactive years (solar minimum) and seven active years (solar maximum). Large SPEs are less frequent than smaller ones that are hard to detect by satellites such as the Geostationary Operational Environmental Satellite system (GOES) in near-Earth orbits. Figure 1 shows the modulation of sunspot numbers (SSN), intensities of galactic cosmic rays (GCR), and GOES recordings in the 22, 23, and 24 cycles. Though multiple instruments have been deployed at various locations in the heliosphere to record the particle composition and energy spectra of SPEs, the series of GOES satellites are particularly useful to analyze SPEs directed to the Earth. Since 1975, 16 GOES satellites have been launched into geostationary orbit above the Earth at geosynchronous altitude ( $\approx 6.6$  Earth radii) where the geomagnetic effects are minor for protons  $\geq 10$  MeV. The fluxes depicted in Figure 1 of P3, P5, and P7 are of the protons in the energy levels  $>11.6$ ,  $>63.1$ , and  $>433$  MeV, respectively. These records clearly show the correlation between the frequency of noticeable SPEs and SSN, GCR, X-ray power, and magnetic measurement.

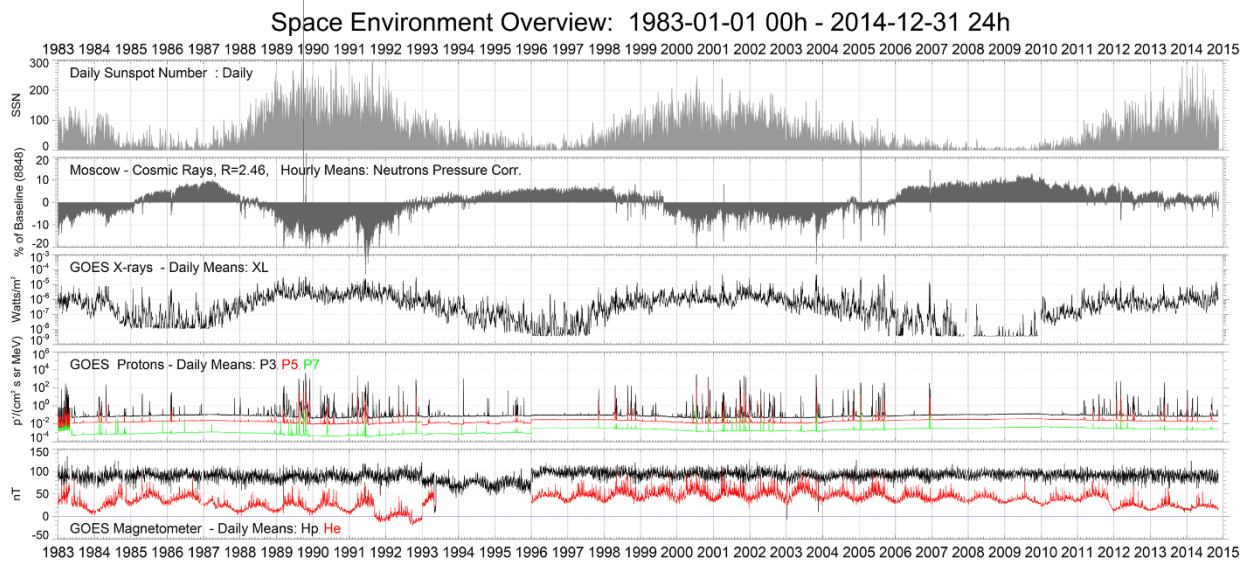


Figure 1. An overview of three solar cycles shows the relationship between the sunspot cycle, galactic cosmic rays, and the state of our near-space environment<sup>2</sup>.

The flux of soft X-rays measured on the GOES spacecraft has been used to classify the size of SPEs. Many observed SPEs are classified as A, B, C, M or X according to the peak flux ( $W/m^2$ ) of 100 to 800 picometer X-rays. Each class has a peak flux 10 times greater than the preceding one, with X class flares having a peak flux of order  $10^{-4} W/m^2$ . Within a class there is a linear scale from 1 to 9, so an X2 flare is twice as powerful as an X1 flare, and is 4 times as powerful as an M5 flare. The more powerful M and X class flares are often associated with a variety of effects on the near-Earth space environment such as the disruption of the Earth's magnetosphere and strong aurora in the pole regions. Besides these X-rays, a spectrum of radio emission like the bremsstrahlung or synchrotron emission of electrons are associated with SPEs [Reames, 2013].

However, many proton dominated SPEs do not show characteristic X-rays or radio emission. Among the 1,265 SPEs with sufficient fluence of proton energy  $>10$  MeV during 1975- 2006, only

<sup>1</sup> [https://sohowww.nascom.nasa.gov/publications/ESA\\_Bull126.pdf](https://sohowww.nascom.nasa.gov/publications/ESA_Bull126.pdf)

<sup>2</sup> [https://satdat.ngdc.noaa.gov/sem/goes/data/new\\_plots/special/Overview\\_19830101-00h\\_20141231-24h.png](https://satdat.ngdc.noaa.gov/sem/goes/data/new_plots/special/Overview_19830101-00h_20141231-24h.png)

673 are reliably associated with X-rays flares [Belov *et al.*, 2005]. Direct ion measurement in space is therefore essential to monitor and record SPEs. Beside the GOES series of satellites, a fleet of solar, heliospheric, geospace, and planetary spacecrafts operate simultaneously to understand the dynamics of the solar system<sup>3</sup>. Figure 2 illustrates the >30 MeV solar proton events observed by various spacecraft since the beginning of the 19<sup>th</sup> solar cycle (SC). In the >30 MeV energy range, the most commonly occurring events are those with an omnidirectional fluence in the  $10^5$  to  $10^6$   $\text{cm}^{-2}$  range. The very large events are those 3 orders of magnitude larger – those with fluence  $>1 \times 10^9$   $\text{cm}^{-2}$ , which occur only a few times in a SC, and may not occur in a SC (like SC 21 in Figure 3).

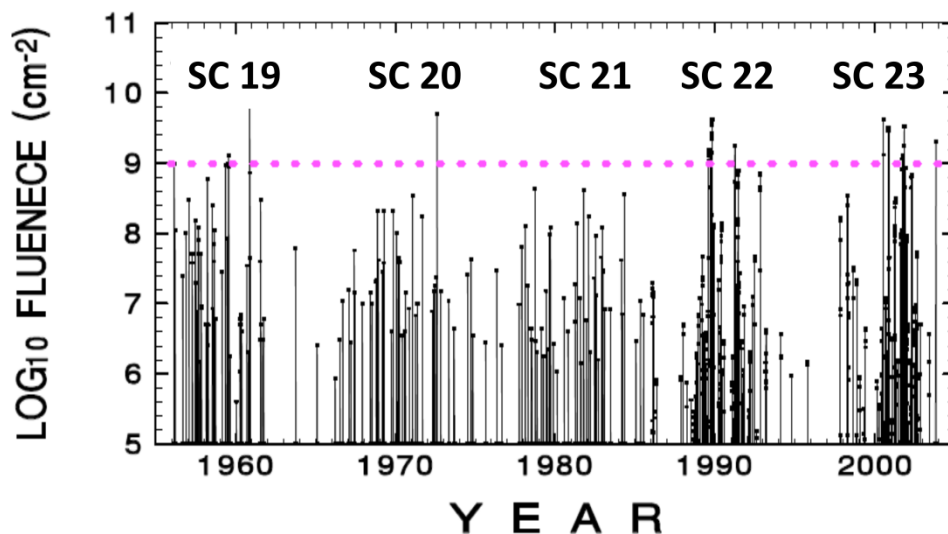


Figure 2. The >30 MeV SPEs since SC 19. The dashed line indicates the  $10^9$   $\text{cm}^{-2}$  omnidirectional solar proton fluence level [Adapted from Smart *et al.*, 2005].

The Carrington event of 1859 is reported in literature as the largest SPE in recent centuries [McCracken *et al.*, 2001]. The omnidirectional fluence of >30 MeV protons in this event is estimated about  $1.88 \times 10^{10}$   $\text{cm}^{-2}$ , which is about 4 times of the August 1972 episode, and about 2.5 times of the November 1960 event. The energetic particles in these large events can usually induce disruption of the Earth's magnetosphere (Figure 1), compressing it on the dayside and extending the night-side tail. While most particles are deflected by Lorentz force due to the magnetosphere and shielded by the atmosphere, protons with energy of ~GeV can create a nuclear cascade through the Earth's atmosphere, which can be observed by detectors at ground level as an increase above the continuous background produced in a similar manner by galactic cosmic rays. These so called ground-level events (GLEs) occurred 71 times in the last 70 years, most barely exceeding the background by a few percentage, the largest by a factor of 45 [Cliver *et al.*, 1982; Reames, 2013].

In addition to direct spacecraft measurement in space, there has been considerable effort to identify signatures of SPEs in such diverse sites as tree rings, polar ice, deep-sea sediments, lunar soils and rocks, and meteorites, in order to quantify the historical frequency and intensity of events.

<sup>3</sup> [https://www.nasa.gov/mission\\_pages/sunearth/missions/index.html](https://www.nasa.gov/mission_pages/sunearth/missions/index.html).

Combined with spacecraft measurements over the last four solar cycles, nitrate analysis in polar ice cores over the past 400 years, radioactivity in moon rocks and meteorites, the very long-term SPE fluence distribution may be represented by a broken power law illustrated in Figure 3 [Reedy, 1996; Smart *et al.*, 2005]. Similar models have been proposed by other researchers [Feynman *et al.*, 1993; Xapsos *et al.*, 1996; Tylka *et al.*, 1997] based on different data sets. These models can be used to estimate the probability of certain level of radiation exposure during an interplanetary mission for risk assessment [NCRP, 2006].

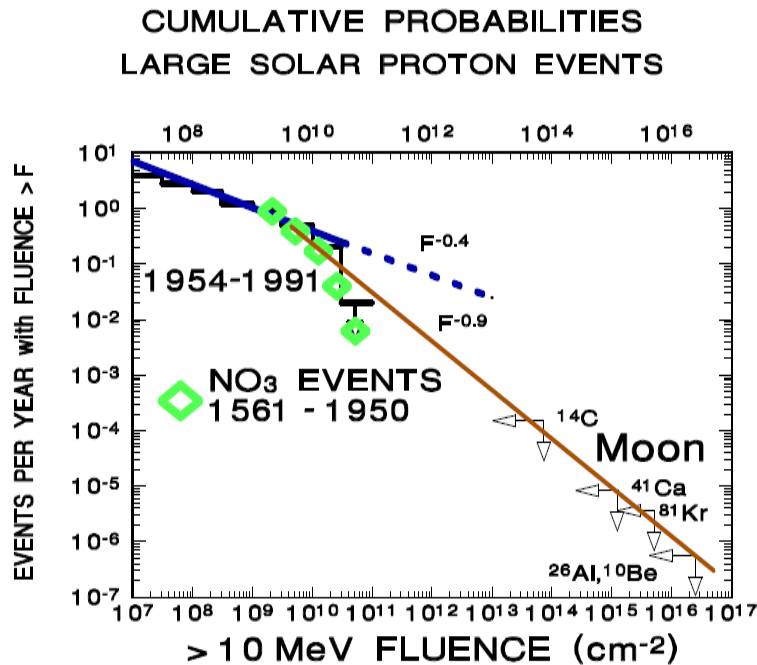


Figure 3. The fluence distribution of Earth-sensed SPEs [Smart *et al.*, 2005].

### 3. SPE Sources and Particle Transport

It is now generally accepted that two types of SPEs occur in our solar system -- impulsive event that is directly related to the solar flares, and gradual event that is caused by CMEs [Desai and Giacalone, 2016]. Solar flares are energetic explosions on the surface of the Sun, occurred when magnetic energy built up in the solar atmosphere is suddenly released. Flares can occur as short impulses that are gone in minutes, or brightenings that decay over hours to days. The impulsive events usually produce a stream of high energy particles that can be observed when the observer is magnetically connected to the flare site (Figure 4), while the slower events are often accompanied by a CME. However, the seed population of a CME can be other sources such as particles in previous CMEs or even solar winds<sup>4</sup>. CMEs are much larger eruptions of the corona at a location up to several solar radii away from the Sun, and the accompanying gradual events involve energetic particles interacting with collisionless-shock waves, propagating in all directions and populating magnetic field lines over a significantly broad range of longitudes (Figure 4). It is

<sup>4</sup> <http://cse.ssl.berkeley.edu/coronalweather/index.html>

now believed that CME-driven coronal and interplanetary shocks are the most prolific producers of SPEs that pose radiation hazards for us, our environment, and our assets on Earth and in space [Reames, 1999].

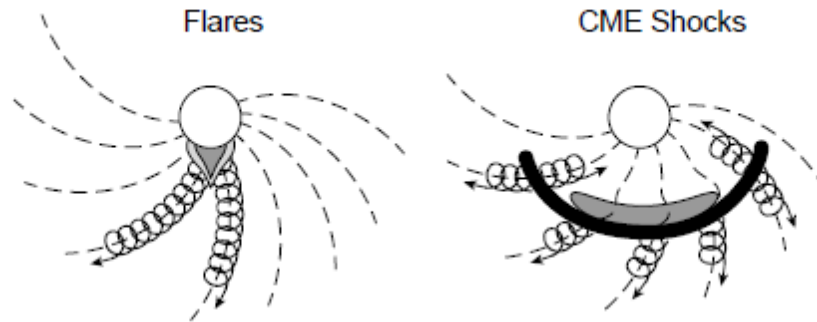


Figure 4. The two-class picture for SPEs where the impulsive event (left) is produced by a solar flare that populates only those interplanetary magnetic field (IMF) lines well-connected to the flare site, and the gradual event (right) is produced by a large-scale CME driven shock wave that accelerates the solar particles and populates IMF lines over a large longitudinal area (adapted from [Reames, 1999]).

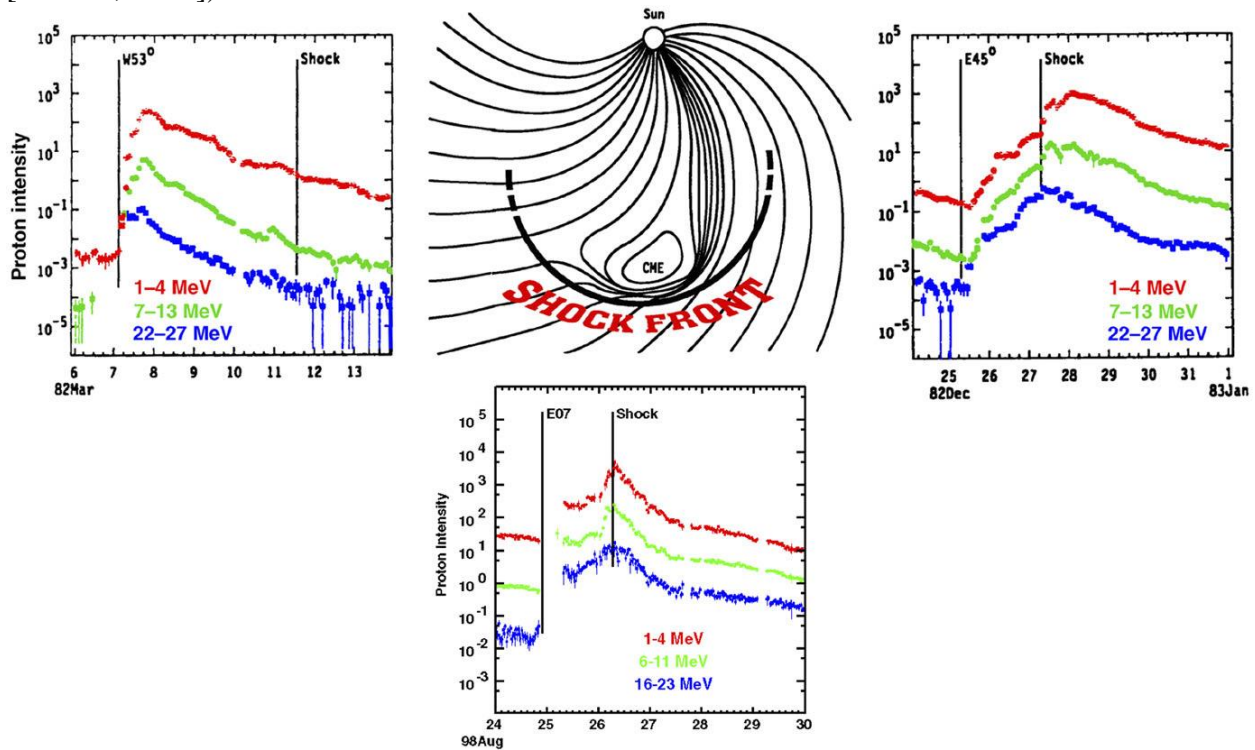


Figure 5. Intensity-time profiles of 1–30 MeV protons during gradual SEP events observed at 3 different solar longitudes relative to the flare or CME lift-off location (adapted from [Cane et al., 1988]).

Though energetic particles in gradual SPEs spread much wider in heliosphere than those in impulsive events, their temporal profiles of intensity vary significantly at different solar longitudes

[Cane *et al.*, 1988]. Analysis of past large SPEs indicates that for events originating from the western hemisphere (right half as observed from the Earth) of the Sun, the Earth-observed proton intensities usually peak earlier than those initiating near the center of the disk, while those with origins from the eastern hemisphere (left half as observed from the Earth) increase much slower and their peaks arrive days later (Figure 5). This can be explained in terms of particles' preferring trajectories along the IMF lines as well as the strongest acceleration occurring near the shock front of CME that moves radially outward from the Sun with time (Figure 5). For observers located east of the source (left panel), as they are magnetically connected to the nose of the CME shock near the Sun, the recorded intensities show abrupt increases and a peak relatively earlier during the event. The intensities decay slowly as the shock moves outward and the magnetic connection shifts to the eastern flanks of the shock. For sources located near the central meridian, the intensities peak when the nose of the shock reaches the location of the observers at a later time (lower panel). In contrast, for observers located to the west (right panel) of the source, they miss the shock front at onset but detect a slow increase in the intensities that peak well after the shock front reaching from the opposite direction to the propagation of the corona mass (Figure 4 right) [Reames, 2013; Desai and Giacalone, 2016].

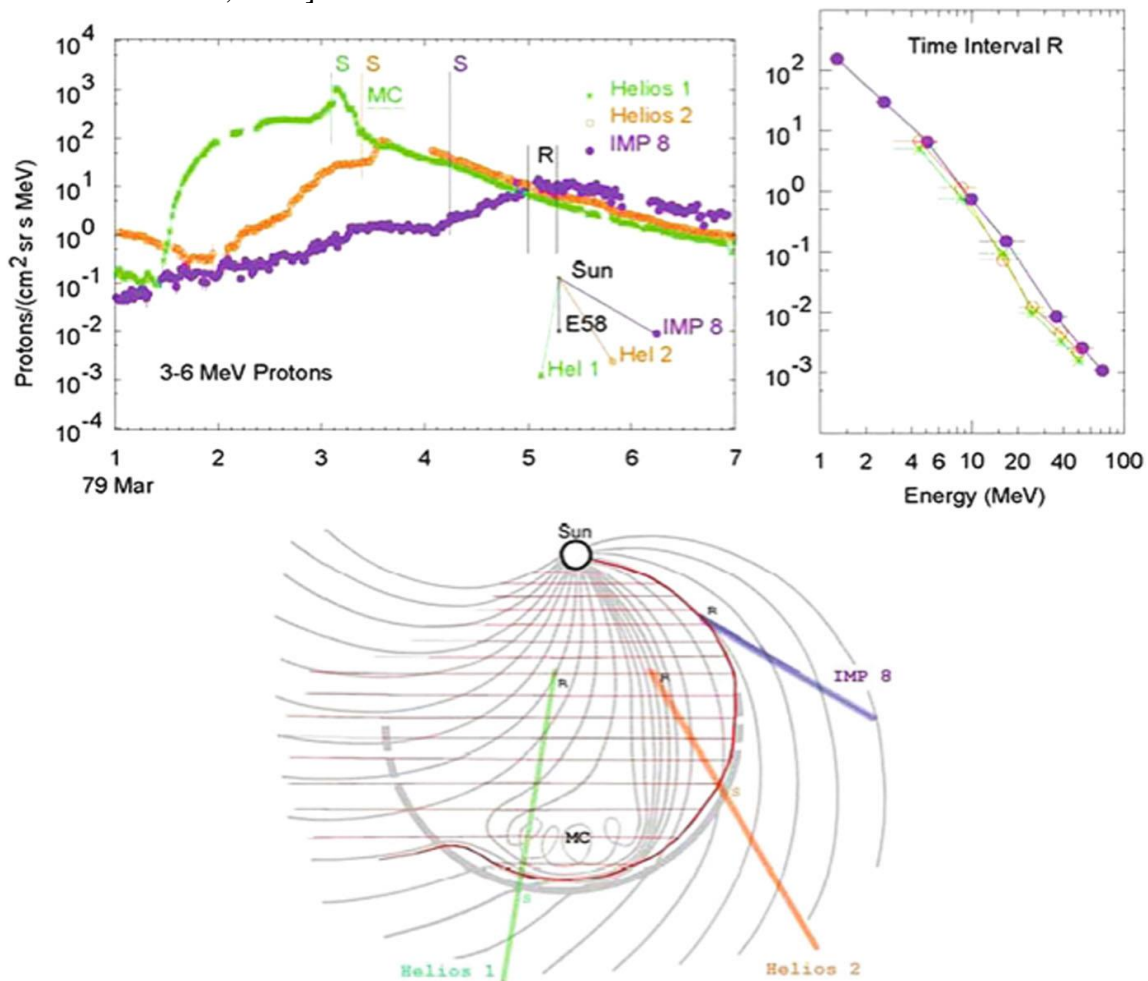


Figure 6. Intensity-time profiles for protons in the 1979 March 1 event at three spacecraft are shown in the upper left panel with times of shock passage indicated by S for each. Helios 1 encounters the event near central meridian and sees an intensity peak of 3-6 MeV protons near

the time of shock passage and subsequently passes through the helical magnetic cloud (MC). Energy spectra in the “reservoir” at time R are shown in the upper right panel while the positions of the spacecraft at time R through a sketch of the CME are shown below [Reames, 2010].

Multiple spacecraft observations also demonstrated the spatial variation of the intensity time-profile of a single event. For the 1979 March 1 event observation depicted in Figure 6, Helios 1 happened to locate at the east side the shock front while Helios 2 and IMP8 were at the west side but at different solar longitudes. The recorded intensities showed the same features as discussed above. However, at a late time point of this event, the intensity profile merged at a same energy level for three detectors at different solar longitudes. The spectra analysis for the time interval “R” indicates the intensities are nearly the same for other energy levels (Figure 6, right panel). This late phase of uniform intensity and spectral shape with overall intensity declining with time was reported as “reservoir” in 1970s [McKibben, 1972], and observed afterwards in many SPEs with wide ranges of azimuthal, radial, and latitudinal locations in the heliosphere [Reames, 2013]. It is now accepted that this type of magnetic reservoirs are created by propagation of solar mass in the IMF, from either gradual events or impulsive events, and energetic particles from nearly any sources can fill it and then gradually leave it [Reames, 2013].

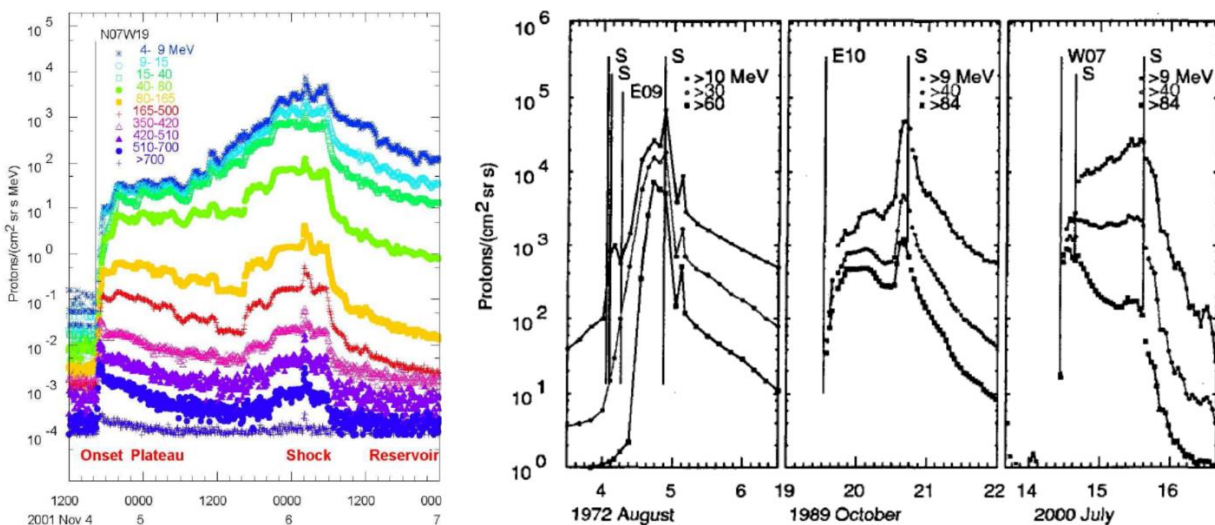


Figure 7. The four phases of a large SPE are indicated along the bottom of the figure showing energetic proton intensities in the 2001 November 4 event (left panel) [Reames, 2013], which can be discerned in other historical SPEs recorded by various instruments near the Earth orbits (right panel) [Reames, 2003]. Times of shock passage are indicated by S for each, while E09, E10, and W07 refer to the origins of the events.

Before this late “reservoir” phase, the time profile of a typical gradual SPE can include the onset, the plateau, and the shock peak as in the 2001 November 4 event depicted in Figure 7 [Reames, 2013]. However, detection of this temporal variation of an event depends on the location of the observer relative to the source, as discussed above. In addition, the pattern of temporal evolution of SPEs varies from event to event (Figure 7). The onset of a gradual event usually involves shock acceleration of the corona materials near the Sun. As protons of a given energy stream away from a shock in a magnetic field, Alfvén waves are generated which scatter protons coming behind and

trap them in the vicinity of the shock. Equilibrium is established between wave amplification and particle scattering, which reduces the streaming and hence the wave growth. Eventually, increasing the source of particles only increases the wave intensity and the scattering with no increase of the outflowing particle intensities seen by a distant observer. This is the streaming limit in the plateau phase that has been observed in many historical SPEs [Reames and Ng, 2014]. It is proposed that the more particles trapped by the streaming limit, the higher the shock peak will be. The wave-particle balance at the shock is lost when the shocks become weak with increasing time, and resonant waves are inadequate to contain the particles of high energy, resulting in the formation of energy spectral knee, i.e., sudden steepening of the particle spectra at high energy [Reames, 2013].

#### 4. SPE Spectra

The spectra of SPEs are used to estimate radiation exposure to astronauts in space, either in the integral format (protons/cm<sup>2</sup>) or differential format (protons/(cm<sup>2</sup>·MeV)). Historically, various analytical functional forms have been applied to fit the satellite data. Due to the limited energy resolution capability of particle detectors in early “Space Age era”, the exponential in particle rigidity fitting method [Malitson and Webber, 1963] has been used in the scientific community for several decades, which is based on two proton integral data points: >30 MeV and >100 MeV. The mathematical expression for the integral energy spectrum is:

$$\Phi(> E) = N_0 \exp\left(-\frac{R}{R_0}\right) \quad (1)$$

where  $\Phi(>E)$  is the integral energy fluence in protons/cm<sup>2</sup>,  $N_0$  is a normalization constant,  $R$  is the proton rigidity (proton momentum) in MV (million volts), and  $R_0$  is the characteristic rigidity in MV. The proton rigidity  $R$  is related to the proton energy (MeV) by:

$$R(MV) = \sqrt{E^2 - 2m_0E} \quad (2)$$

where  $E$  is the proton energy (MeV) and  $m_0$  is the rest mass of the proton (938 MeV) [Atwell *et al.*, 2011]. In literature of SPE modeling, the exponential spectrum is usually extrapolated to the range of 10 MeV to several GeV. A similar scheme of spectrum modeling uses a Weibull function of the following form:

$$\Phi(> E) = \Phi_0 \exp(-kE^\alpha), \quad (3)$$

where parameters  $\Phi_0$ ,  $k$ , and  $\alpha$  are determined by a nonlinear regression fit to the energy spectrum of interest [Xapsos *et al.*, 2000]. A number of SPEs have been analyzed using this approach with maximum energy of 1 GeV [Kim *et al.*, 2009].

A Band functional form of SPE spectrum is getting more attention recently, which is a power law that rolls smoothly into a second, steeper power law, with a functional form that is continuous in both its value and derivative:

$$\begin{aligned} \Phi(> R) &= \Phi_0 R^{-\gamma_1} \exp\left(-\frac{R}{R_0}\right), & \text{if } R \leq (\gamma_2 - \gamma_1)R_0 \\ &= \Phi_0 R^{-\gamma_2} \{[(\gamma_2 - \gamma_1)R_0]^{(\gamma_2 - \gamma_1)} \exp(\gamma_2 - \gamma_1)\}, & \text{if } R > (\gamma_2 - \gamma_1)R_0 \end{aligned} \quad (4)$$

where  $\gamma_1$  and  $\gamma_2$  are the spectral indices for the lower and higher energy branches respectively [Tylka and Dietrich, 2009]. Parameters for the lower energy branch are obtained from satellite data from medium (10-100 MeV) and high (several hundred MeV) proton energies (GOES Energetic Proton, Electron and Alpha Detector (EPEAD) and High Energy Proton and Alpha Detector (HEPAD) and other satellites), while those for the higher energy branch are from cascade secondary neutrons produced during nuclear collisions of the incoming solar protons with the Earth's atmosphere ( $> 1$  GV).

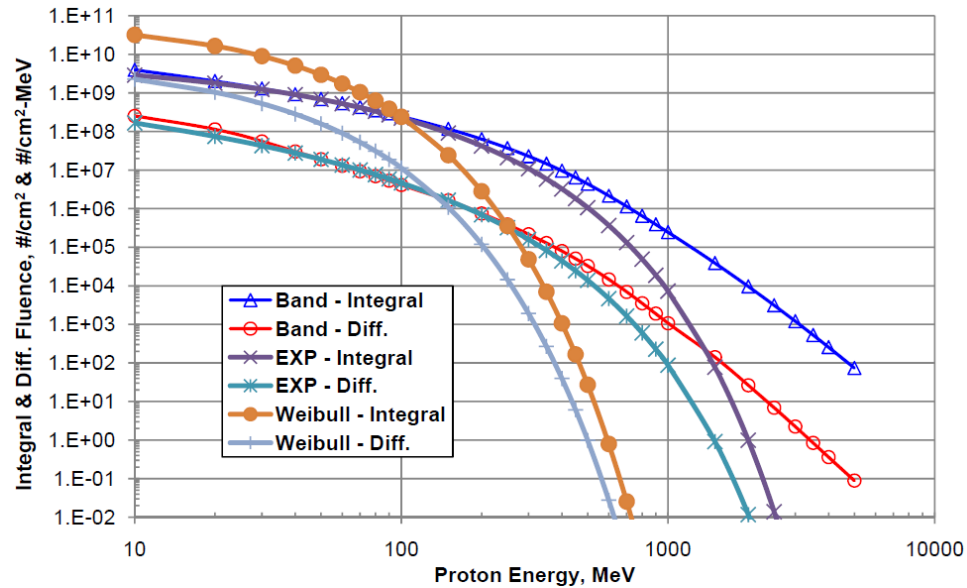


Figure 8. Three functional forms of spectra fitting for the 1960 Nov 12 SPE [Atwell *et al.*, 2011]

A comparison study of 12 GLEs with these three methods has found significant difference in the modeled fluence for a same event [Atwell *et al.*, 2011]. Figure 8 shows that spectra of either Exponential form or Weibull form significantly underestimate the particle intensities at high energies, as compared with Band form which is supported with data from a network of neutron monitoring stations at the high latitudes on the Earth. As the protons in the high energy range contribute the most in radiation effects, it seems necessary to revisit the spectra and radiation exposure modeling of past SPEs reported in literature by applying this new formalism.

A recent analysis of GOES MEPAD and HEPAD data indicates that Band functional form can be approximated by a segmental power law fitting algorithm [Hu *et al.*, 2016]. Directly using the differential fluence at the defined energy grids, the interpolated segmental spectra of several GLEs are very close to their reported spectra in Band functional form, from energy  $< 10$  MeV to several GeV. This algorithm does not use the ground neutron monitors data, as the directly streamed data from GOES HEPAD are found to be sufficient to model the high energy branch of spectra, as long as the recorded intensities by these detectors are large enough (true for all GLEs). For many SPEs, the fluences of high energy protons may be too small to be measured by GOES, and the algorithm ensures a cutoff at the respective energy grid, therefore avoiding erroneous extrapolation of the spectra to higher energy range [Hu *et al.*, 2016].

It has been reported that spectra of many SPEs do not follow any specific functional forms due to the intrinsic characteristics of particle acceleration and propagation in interplanetary space. The spectra of ions shown in the left panel of Figure 9 have peaks at  $\sim 10$  MeV  $\text{amu}^{-1}$  and roll downward toward lower energies, which are proposed to be induced by the streaming limits as discussed previously, i.e., high intensities of streaming particles at  $\sim 10$  MeV produce waves that suppress the spectra at  $\sim 1$  MeV [Reames, 2013]. On the other hand, for the hourly fluences of protons displayed in the right panel, peaks for protons with energies  $>50$  MeV appear at the third hour from onset, while the peaks for protons with lower energies follow hours later. This early arrival of high-energy protons is normal for many SPEs [Smart and Shea, 1999], as protons with higher energy are less interrupted by the interplanetary media and heliomagnetic field [Miroshnichenko, 2015]. The segmental power law interpolating scheme is more suitable than the Band function to handle these peculiar cases. To generate the full spectra, this scheme just sequentially interpolates between the measured data points and links to the high-energy branches fitted with the HEPAD data points [Hu et al., 2016].

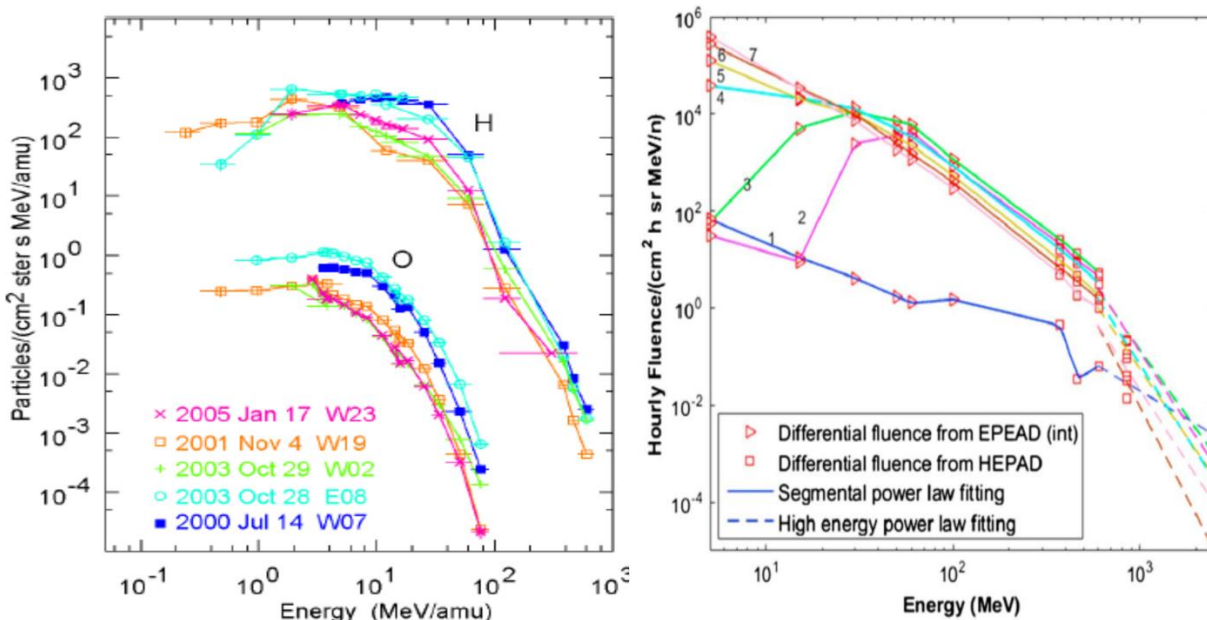


Figure 9. Shapes of spectra that defy any analytical functional forms. The left panel shows H and O spectra for the early plateau region of 5 large SPEs [Reames and Ng, 2010], and the right one shows hourly spectra of 2012 May 17 event after onset, from 0100 to 0700 UTC (denoted by numbers), approximated by a segmental power law fitting algorithm [Hu et al., 2016].

## 5. Radiation Exposure Modeling

While particles of low energies are usually blocked off by minimal shielding, those with energy  $>50$  MeV can penetrate spacesuits and the skin of spacecraft. The physical description of the transmission of high-energy particles through matter is complicated, but the dominant processes include energy loss through atomic and molecular collision and the absorption and particle production from nuclear interaction with spacecraft material and tissue, which can be modeled

using transport equations [NCRP, 2006]. Alternatively, Monte-Carlo codes such as GEANT, HETC, and FLUKA can be used which sample from interaction processes for individual primaries or their secondaries to develop histories of charged particle passage and energy deposition in materials [NCRP, 2006]. Given an event spectrum or temporal profile of spectra of an event, either way can provide physical quantities of radiation exposure to astronauts and instruments in space. These quantities can be used in biological or physical response models to assess the impacts of SPEs to space missions.

To assess acute radiation risks due to SPE exposures, NASA has developed an Acute Radiation Risk and BRYNTRN Organ Dose (ARRBOD) projection code [Kim *et al.*, 2010]. In this software package some historical intense SPEs are analyzed with the transport code BRYNTRN [Cucinotta *et al.*, 1995; Wilson *et al.*, 1989] and ray tracing techniques with human phantom models, so that dosimetric quantities for various organs can be obtained for astronauts during transition and on planetary surfaces for lunar or Mars missions. If the astronauts encountered an SPE event, the resultant organ doses are then used to estimate the severity of possible effects of acute radiation sickness (ARS), such as prodromal effects including nausea, vomiting, fatigue, and weakness [Anno *et al.*, 1989; Hu *et al.*, 2009], and various hematopoietic responses [Hu and Cucinotta, 2011; Hu *et al.*, 2012]. NASA mission planners, radiation shield designers, operational supporters, and space biophysics researchers can use this tool to appreciate the clinically significant deterministic health effects, as well as the degradation of in-flight performance of astronauts, from exposure to large SPEs [Kim *et al.*, 2010].

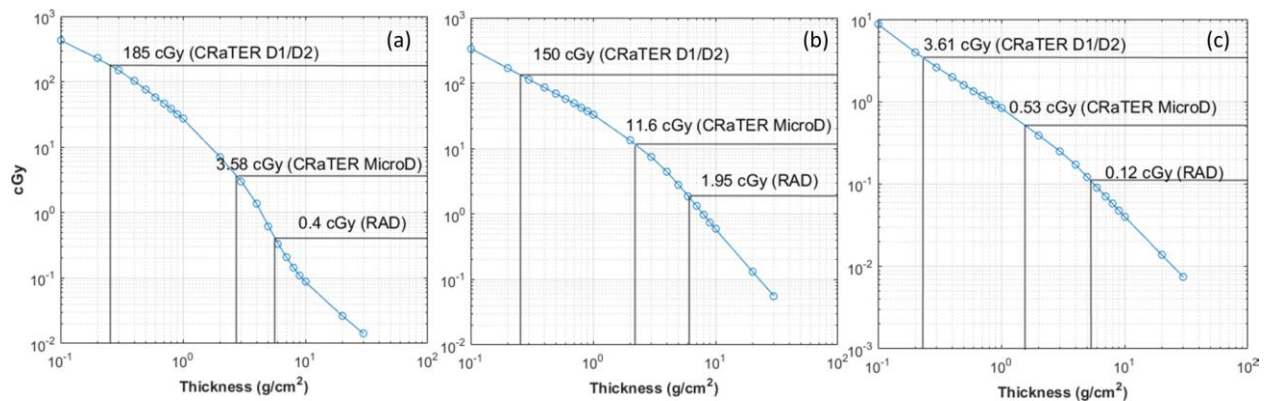


Figure 10. Comparison of total exposure calculated from hourly fluences and recorded with in situ measurements. The three events are 2012-Jan-23 (a), 2012-Mar-7 (b), and 2012-May-17 (c) [Hu *et al.*, 2016].

This idea has recently extended by using the segmental fitting algorithm and HZETRN modeling [Hu *et al.*, 2016]. In this work dosimetric quantities of three SPEs in 2012 are calculated and compared with in situ measurement by two detectors specifically designed for radiation exposure measurement in space. The three SPEs 2012-Jan-23, 2012-Mar-7, and 2012-May-17 happened to be recorded by the Radiation Assessment Detector (RAD) inside the Mars Science Laboratory (MSL) spacecraft during its cruise to Mars [Zeitlin *et al.*, 2013]. They were also recorded by the Cosmic Ray Telescope for the Effects of Radiation (CRaTER), an instrument on the Lunar Reconnaissance Orbiter (LRO) spacecraft designed to characterize the lunar radiation environment. Figure 10 shows the total doses of the three events in a silicon detector behind

aluminum shielding of different thicknesses, compared with published results of in situ measurement during these events [Joyce *et al.*, 2013; Zeitlin *et al.*, 2013]. The doses recorded by CRaTER detectors D1/D2 consistently fall between the modeled doses for 0.2 and 0.3 g/cm<sup>2</sup> shielding (Figure 5), which is in accordance with the 0.22 g/cm<sup>2</sup> thickness of the telescope cap [Mazur *et al.*, 2011]. The CRaTER microdosimeter (MicroD) doses are a bit more scattered, falling between the modeled doses for 1 and 3 g/cm<sup>2</sup> thicknesses of shielding (Figure 10). Though the recorded dose for the May SPE is a bit less than the modeled dose for 2 g/cm<sup>2</sup> shielding (Figure 10c), overall the results for these events are reasonably compatible with the 2.28 g/cm<sup>2</sup> thickness of the shielding for this detector [Mazur *et al.*, 2011]. This consistency also holds for the RAD doses, which fall between the modeled doses for 5 and 6 g/cm<sup>2</sup> (Figure 10). This agreement between modeling and in situ measurement is remarkable, as the shielding configuration of each detector is complex, the orientation and position of the spacecraft in space are always changing, and the radiation environment of the different events is not exactly the same [Joyce *et al.*, 2013].

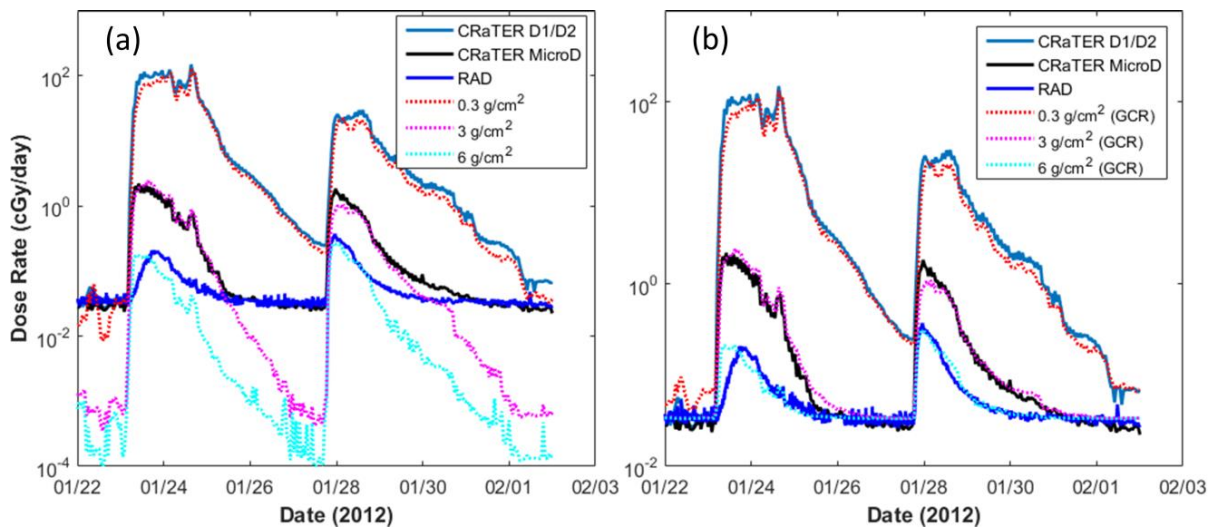


Figure 11. Dose rates of the January SPE determined by in situ measurement and model calculation. (a) Comparison of in situ measurement and modeled dose rates from segmental hourly fluences. (b) Comparison of in situ measurement and modeled dose rates plus galactic cosmic ray background (0.022 cGy/day) [Hu *et al.*, 2016].

Figure 11a shows the dose rates measured by CRaTER and RAD during the 2012 January SPE, as well as modeling simulations from the hourly spectra behind aluminum shielding of different thicknesses. The modeled dose rates with 0.3 g/cm<sup>2</sup> shielding are in good agreement with CRaTER D1/D2 measurement, except in the periods before the onset and near the end of each of the two subevents. The modeled 3 g/cm<sup>2</sup> dose rates are in excellent agreement with those from the CRaTER microdosimeter at the first peak and at certain times after the second, but have large discrepancies whenever the measured dose rates fall below 0.1 cGy/day (Figure 11a). This trend is also observed for the modeled 6 g/cm<sup>2</sup> dose rates and the RAD measurements (Figure 11a). After simply adding the background GCR dose rates during the course of this event, almost all the discrepancies are removed as demonstrated in Figure 11b. Adding the background dose rates did not modify the comparison during the peak periods when the measured and modeled dose rates were high, but it significantly elevated the modeled dose rates when proton fluxes were low, either

before the onset or near the end of each of the two subevents (Figure 11b). As the background proton fluxes are removed from GOES data in this algorithm, however they are ubiquitously recorded along with other species of GCR by in situ instruments, the achieved agreement is indeed not a surprise.

This work demonstrates that omnipresent GCRs are an important component in modeling the temporal profile of radiation exposure during an SPE, as simply adding the GCR effects also significantly corrected the discrepancies between modeled dose rates and in situ measurements for the 2012 March and May SPEs [Hu *et al.*, 2016]. Because during a severe SPE not only protons but also high energetic electrons, alpha particles, and heavier particles contribute to the exposure of certain critical tissues and have important implications for the models of risk assessment [Kim *et al.*, 1999], a full comparison with in situ measurements is more rational if all the sources (including SPE and GCR) are considered in the input spectra for transport calculation. A necessary next step for further development of SPE modeling will be adding a module for fitting the intensity of incident alpha particles, which may contribute 10%-40% of the total dose during a severe SPE [Kim *et al.*, 1999]. Additionally, the background GCR dose rates can be replaced with transport calculations behind realistic shielding structures with validated GCR models [Badhwar and O'Neill, 1992; O'Neill, 2010], so that the health effects of the breakup of the heavy ions into lighter components, including neutrons, can be fully investigated.

## 6. Summary

This article summarizes recent observations and theoretical frameworks concerning on the origin, acceleration, and transport of energetic particles in SPEs, and reviews knowledge of the size, frequency, energy spectrum of SPE, as well as techniques of radiation exposure modeling relevant to interplanetary space exploration.

## References

- Anno, G. H., S. J. Baum, H. R. Withers, R. W. Young (1989), Symptomatology of acute radiation effects in humans after exposure to doses of 0.5–30 Gy, *Health Phys.*, 56, 821–838.
- Atwell, W., A. Tylka, W. Dietrich, F. Badavi, K. Rojdev (2011), Spectral analyses and radiation exposures from several ground-level enhancement (GLE) solar proton events: a comparison of methodologies, presented at 41st International Conference on Environmental Systems, International Conference on Environmental Systems (ICES), Portland, Oregon, July 17-21
- Badhwar, G. D. and P. M. O'Neill (1992), An improved model of GCR for space exploration missions, *Nucl. Tracks Radiat. Meas.*, 20, 403-410.
- Belov, A., H. Garcia, V. Kurt, H. Mavromichalaki, M. Gerontidou (2005), Proton enhancements and their relation to the X-ray flares during the three last solar cycles, *Sol. Phys.*, 229, 135-159.
- Cane, H. V., D. V. Reames, T. T. von Roseninge (1988), The role of interplanetary shocks in the longitude distribution of solar energetic particles, *J. Geophys. Res.* 93, 9555–9567.
- Cliver, E. W., S. W. Kahler, M. A. Shea, D. F. Smart (1982), Injection onsets of 2 GeV protons, 1 MeV electrons and 100 keV electrons in solar cosmic ray flares. *Astrophys. J.*, 260, 362–370.

- Cucinotta, F. A., J. W. Wilson, and F. A. Badavi (1995), Extension of the BRYNTRN code to Monoenergetic Light Ion Beams, NASA Technical Paper 3472. NASA Langley Research Center, Hampton, VA
- Desai, M. and J. Giacalone (2016), Large gradual solar energetic particle events, *Living Rev. Sol. Phys.*, 13:3.
- Feynman, J., G. Spitale, J. Wang, S. Gabriel (1993), Interplanetary proton fluence model, *J. Geophys. Res.*, 98, 13281-13294.
- Hu, S. and F. A. Cucinotta (2011), Characterization of the radiation-damaged precursor cells in bone marrow based on modeling of the peripheral blood granulocytes response, *Health Phys.*, 101(1), 67-78.
- Hu, S., M-H. Y. Kim, G. E. McClellan, F. A. Cucinotta (2009), Modeling the acute health effects of astronauts from exposure to large solar particle events, *Health Phys.*, 96(4), 465-476.
- Hu, S., O. A. Smirnova, F. A. Cucinotta (2012), A biomathematical model of lymphopoiesis following severe radiation accidents — potential use for dose assessment, *Health Phys.*, 102(4), 425-436.
- Hu, S., C. Zeitlin, W. Atwell, D. Fry, J. E. Barzilla, E., Semones (2016), Segmental interpolating spectra for solar particle events and in situ validation, *Space Weather*, 14, doi:10.1002/2016SW001476
- Joyce, C. J., N. A. Schwadron, J. K. Wilson, H. E. Spence, J. C. Kasper, M. Golightly, J. B. Blake, J. Mazur, L.W. Townsend, A. W. Case, E. Semones, S. Smith, C. J. Zeitlin (2013), Validation of PREDICCS using LRO/CRaTER observations during three major solar events in 2012, *Space Weather*, 11, 350–360, doi:10.1002/swe.20059.
- Kim, M-H. Y., J. W. Wilson, F. A. Cucinotta, L. C. Simonsen, W. Atwell, F. F. Badavi, J. Miller (1999), Contribution of high charge and energy (HZE) ions during solar particle event of September 29, 1989, NASA/TP-1999-209320. NASA Langley Research Center, Hampton, VA
- Kim, M-H. Y., M. J. Hayat, A. H. Feiveson, F. A. Cucinotta (2009), Prediction of frequency and exposure level of solar particle events, *Health Physics*, 97, 68-81.
- Kim, M-H. Y., S. Hu, H. N. Nounu, F. A. Cucinotta (2010), Development of graphical user interface for ARRBOD (Acute Radiation Risk and BRYNTRN Organ Dose projection). Hanover, MD: Center for Aerospace Information; NASA TP-2010-216116.
- Malitson, H. H. and W. R. Webber (1963), A summary of solar cosmic ray events, in *The Solar Proton Manual*, NASA TR R-169, Washington D. C.
- Mazur, J. E., W. R. Crain, M. D. Looper, D. J. Mabry, J. B. Blake, A. W. Case, M. J. Golightly, J. C. Kasper, H. E. Spence (2011), New measurements of total ionizing dose in the lunar environment, *Space Weather*, 9, S07002, doi:10.1029/2010SW000641.
- McCracken, K. G., G. A. M. Dreschhoff, E. J. Zeller, D. F. Smart, M. A. Shea (2001a), Solar cosmic ray events for the period 1561-1994. 1. Identification in polar ice, 1561-1950, *J. Geophys. Res.*, 106(A10), 21,585-21,598.
- McKibben, R. B. (1972), Azimuthal propagation of low-energy solar-flare protons as observed from spacecraft very widely separated in solar azimuth, *J. Geophys. Res.*, 77(2), 3957-3984.
- Miroshnichenko, L. (2015), *Solar Cosmic Rays: Fundamentals and Applications*, Springer, New York.
- NCRP (2006). NCRP Report No. 153. Information Needed To Make Radiation Protection Recommendations for Space Missions Beyond Low-Earth Orbit. Bethesda, MD, NCRP.
- O'Neill, P. M. (2010), Badhwar–O'Neill 2010 galactic cosmic ray flux model: Revised, *IEEE Trans. Nucl. Sci.*, 57(6), 3148–3153.

- Reames, D.V. (1999), Particle acceleration at the Sun and in the heliosphere, *Space Science Reviews*, 90, 413-491.
- Reames, D. V. (2003), Solar energetic particle variations, *Adv. Space Res.*, 34, 381 – 390.
- Reames, D. V. (2010), Remote sensing of magnetic-cloud topology, *Sol. Phys.*, 265, 187–195.
- Reames, D. V. (2013), The two sources of solar energetic particles, *Space Sci. Rev.*, 175, 53–92.
- Reames, D. V. and C. K. Ng (2010), Streaming-limited intensities of solar energetic particles on the intensity plateau, *Astrophys. J.* 723, 1286–1293.
- Reames, D. V. and C. K. Ng (2014), The streaming limit of solar energetic-particle intensities, presented at Extreme Space Weather Events in Boulder, Co, June 9-11.
- Reedy, R. C. (1996), Constraints on solar particle events from comparisons of recent events and million-year averages, in *Solar Drivers of Interplanetary and Terrestrial Disturbances*, edited by K.S. Balasubramanian, S.L. Keil, and R.N. Smartt. *Astronomical Society of the Pacific, Conference Series*, 95, 429-436.
- Smart, D. F. and M. A. Shea (1999), Comment on the use of GOES solar proton data and spectra in solar proton dose calculations, *Radiation Measurements*, 30, 327-335.
- Smart D. F., M. A. Shea, G. A. M. Dreschhoff, H. E. Spence, L. Kepko (2005), The frequency distribution of solar proton events: 5 solar cycles and 45 solar cycles, presented in the Conference of Solar and Space Physics and the Vision for Space Exploration, Wintergreen Resort, VA, 16-20 October
- Tylka, A. J., W. F. Dietrich, P. R. Bobery (1997), Probability distributions of high-energy solar-heavy-ion fluxes from IMP-8: 1973-1996, *IEEE Trans. Nucl. Sci.*, 44(6), 2140-2149.
- Tylka, A. J. and W. F. Dietrich (2009), A new and comprehensive analysis of proton spectra in ground-level enhanced (GLE) solar particle events, *Proceedings of the 31st International Cosmic Ray Conference*, Lodz, Poland, Universal Academy Press.
- Wilson, J. W., et al. (1989), BRYNTRN: A Baryon transport model, *NASA Report No. TP-2887*, Washington, D.C.
- Xapsos, M. A., G. P. Summers, P. Shapiro, E. A. Burke (1996), New techniques for predicting solar proton fluences for radiation effects applications, *IEEE Trans. Nucl. Sci.*, 43(6), 2772-2777,
- Xapsos, M. A., et al. (2000), Characterizing solar proton energy spectra for radiation effects applications, *IEEE Trans. Nucl. Sci.*, 47(6), 2218–2223.
- Zeitlin, C., et al. (2013), Measurements of energetic particle radiation in transit to Mars on the Mars science laboratory. *Science*, 340, 1080-1084.